第 34 卷第 11 期 无 机 化 学 学 报 Vol.34 No.11
2018 年 11 月 CHINESE JOURNAL OF INORGANIC CHEMISTRY 1950-1965

光催化剂 Sm_2FeSbO_7 的制备及光物理和光催化性能表征

栾景飞* 谭文成
(南京大学环境学院污染控制与资源化研究国家重点实验室,南京 210023)

摘要:首次采用固相反应法制备了新型光催化剂 Sm_2FeSbO_7,有效地降解了水中有机污染物。利用 X 射线衍射、扫描电镜、X 射线光电子能谱、傅里叶变换红外光谱、透射电子显微镜和紫外-可见光谱仪对 Sm_2FeSbO_7 的结构和光催化性能进行了表征。Sm_2FeSbO_7 为烧绿石型结构,立方晶系和空间群 *Fd*3*m* 结晶。Sm_2FeSbO_7 的晶格参数 *a* 为 1.035 434 nm。Sm_2FeSbO_7 的带隙经估算为 2.46 eV。用 Sm_2FeSbO_7 作为光催化剂在可见光照射下降解靛蓝胭脂红,并与氮掺杂 TiO_2 对比。结果表明,与掺氮 TiO_2 相比,Sm_2FeSbO_7 在可见光照射下光催化降解靛蓝胭脂红显示出较高的光催化活性。总有机碳的减少,无机产物的逐渐形成,SO_4^{2-}和 NO_3^-以及 CO_2 的演变揭示了在光催化过程中靛蓝胭脂红的连续矿化。检测了一些来自光催化降解靛蓝胭脂红的中间体,如邻硝基苯甲酸和邻硝基苯甲醛,并获得了可能的靛蓝胭脂红光催化降解路径。

关键词:催化作用; Sm_2FeSbO_7; 光催化降解; 可见光照射; 光降解路径; 靛蓝胭脂红
中图分类号:O643.36 **文献标识码**:A **文章编码**:1001-4861(2018)11-1950-16
DOI:10.11862/CJIC.2018.245

Preparation, Photophysical and Photocatalytic Property Characterization of Sm_2FeSbO_7 during Visible Light Irradiation

LUAN Jing-Fei* TAN Wen-Cheng
(*State Key Laboratory of Pollution Control and Resource Reuse, School of the Environment, Nanjing University, Nanjing* 210023, *China*)

Abstract: In order to efficiently degrade organic pollutants in water, a new photocatalyst Sm_2FeSbO_7 was prepared by a solid-state reaction method for the first time. The construction and photocatalytic property of Sm_2FeSbO_7 had been characterized by X-ray diffraction, scanning electron microscopy, X-ray photoelectron spectroscopy, Fourier-transform infrared spectroscopy, transmission electron microscope and UV-visible spectrometer. Sm_2FeSbO_7 crystallized with a pyrochlore-type structure, a cubic crystal system and a space group *Fd*3*m*. The lattice parameter *a* of Sm_2FeSbO_7 was 1.035 434 nm. The band gap of Sm_2FeSbO_7 was estimated to be 2.46 eV. The photocatalytic degradation of indigo carmine was accomplished under visible light irradiation with Sm_2FeSbO_7 as a catalyst compared with nitrogen-doped TiO_2. The results indicated that Sm_2FeSbO_7 displayed higher photocatalytic activity compared with nitrogen-doped TiO_2 for the photocatalytic degradation of indigo carmine under visible light irradiation. The reduction of the total organic carbon, the gradual formation of inorganic products, SO_4^{2-} and NO_3^-, and the evolution of CO_2 revealed the continuous mineralization of indigo carmine during the photocatalytic process. Some intermediate products which came from the photocatalytic degradation of indigo carmine were detected, such as o-nitrobenzoic acid and o-nitrobenzaldehyde, and a possible photocatalytic degradation path of indigo carmine was acquired.

Keywords: catalysis; Sm_2FeSbO_7; photocatalytic degradation; visible light irradiation; photodegradation pathway; indigo carmine

收稿日期:2018-05-17。收修改稿日期:2018-08-14。
第 5 批中国-以色列科学与战略研究开发基金项目(No.[2010]30)和国家自然科学基金(No.21277067)资助。
*通信联系人。E-mail:jfluan@nju.edu.cn

0 Introduction

Coloring matter wastewater in the textile and photographic industries had become a serious environmental problem due to its toxicity, unacceptable color, high chemical oxygen demand, and biodegradability[1]. The presence of dyes in water was not only aesthetically unpleasant, but it also affected the transparency of water, decreased sun penetration, reduced gas solubility, and photosynthetic reactions[2]. For the sake of solving the problem, many scientists hope to use photocatalytic techniques to degrade harmful coloring matter wastewater from polluted water before proper treatment, and these scientists had made different efforts for this career for more than 40 years[3-5]. At present, photocatalytic degradation process had been widely used in the demolishment of organic pollutants in wastewater, especially the degradation of coloring matter[6].

The selection of the wavelength of the incident light was crucial for the photocatalytic degradation system, while light was a presence of energy. Previous studies had shown that the semiconductor compounds could break down most persistent organic pollutants such as coloring matter, pesticides, detergents and volatile organic compounds under ultraviolet light irradiation[7-10] and had higher energy than visible light.

According to the data, ultraviolet light accounted for only 4% of sunlight, while visible light accounted for about 43%. Thus it seemed more practical and significant to use visible light instead of UV light during the degradation process. Therefore, there was an urgent demand to develop new photocatalysts that responded to visible light and had higher photocatalytic efficiency. In general, most of the photocatalytic catalysts utilized in previous studies were mainly sorted into two types: one was called TiO_2-based catalyst whose maximum absorption wavelength had been extended to visible light by ion doping[11-20] and cocatalyst recombination[21-31], and the other was a complex oxide, such as La_2O_3, $BiVO_4$, $Bi_{12}TiO_{20}$, $K_6Nb_{10.8}O_{30}$[32-38]. Recently, spinel-type oxides having the formula AB_2O_4 had been found to own excellent properties for degrading coloring matter in wastewater under visible light irradiation. For instance, MIn_2O_4 (M=Ca, Sr, Ba)[11,39,40], $NiCo_2O_4$[11] and $ZnFe_2O_4$/MWCNTs[41] were prepared under visible light irradiation. In addition, $ZnFe_2O_4$ owned outstanding property for degradation of methyl orange[42].

In this paper, a new type of semiconductor catalyst Sm_2FeSbO_7 which belonged to the $A_2B_2O_7$ family was prepared. Indigo carmine (IC) was utilized as a model contaminant to evaluate the degradation activity of Sm_2FeSbO_7 under visible light irradiation because of its wide use and hard biodegradation. In addition, the construction and photocatalytic characterization of Sm_2FeSbO_7 were also investigated in detail. For comparison, we chose the traditional photocatalyst N-doped TiO_2 (N-TiO_2) to degrade IC under visible light irradiation.

1 Experimental

1.1 Synthesis of nanocatalyst

The new photocatalyst, Sm_2FeSbO_7 was prepared by the solid-state reaction method. Sm_2O_3, Fe_2O_3 and Sb_2O_5 with a purity of 99.99% (Sinopharm Group Chemical Reagent Co., Ltd., Shanghai, China) were used as original materials. For the sake of synthesizing Sm_2FeSbO_7, the precursors were stoichiometrically mixed in a quartz mortar, then transfered into small columns and put into an alumina crucible (Shenyang Crucible Co., Ltd, Shenyang, China). And next, calcination was carried out at 800 ℃ for 35 h in an electric furnace (KSL 1700X, Hefei Kejing Materials Technology Co., Ltd, Hefei, China). The last step was sintering and grinding with a quartz mortar, and then, Sm_2FeSbO_7 powder was made. All powders were dried at 200 ℃ for 4 h before they were prepared. Nitrogen-doped titania (N-TiO_2) catalyst with tetrabutyl titanate as a titanium precursor was prepared by using the sol-gel method at room temperature. The next step was that 17 mL tetrabutyl titanate and 40 mL absolute ethyl alcohol were mixed as solution A; subsequently, solution A was added dropwise under vigorous stirring into the solution B which contained 40 mL absolute ethyl alcohol, 10 mL glacial acetic acid and 5 mL

double distilled water to form transparent colloidal suspension C. Subsequently, aqua ammonia with N/Ti proportion of 8% (*n*/*n*) was added into the resulting transparent colloidal suspension under vigorous stirring condition and stirred for 1 h. Finally, the xerogel was formed after being aged for 2 days. The xerogel was ground into powder, which was calcinated at 500 ℃ for 2 h; and next, above powder was ground in an agate mortar and screened by a shaker to obtain N-doped TiO_2 powders.

1.2 Characterization of Sm_2FeSbO_7

The particle formation of Sm_2FeSbO_7 were measured by transmission electron microscope (TEM, Tecnal F20 S-Twin, FEI Corporation, Hillsboro, Oregon, USA) with 200 kV operating voltage. The chemical ingredient of the compound was determined by a scanning electron microscope with 20 kV operating voltage, which was equipped with X-ray energy dispersion spectrum (SEM-EDS, LEO 1530VP, LEO Corporation, Pegnitz, Germany) and X-ray photoelectron spectroscopy (XPS, ESCALABMK-2, VG Scientific Ltd., East Grinstead, UK). The Sm^{3+}, Fe^{3+}, Sb^{5+} and O^{2-} content of Sm_2FeSbO_7 and the valence state of the elements were also analyzed by X-ray photoelectron spectroscopy. The chemical ingredient within the depth profile of Sm_2FeSbO_7 was examined by the argon ion denudation method when X-ray photoelectron spectroscopy was utilized. The crystalline phase of Sm_2FeSbO_7 was analyzed by X-ray diffractometer (D/MAX-RB, Rigaku Corporation, Tokyo, Japan) with Cu $K\alpha$ radiation (λ=0.154 056 nm). The patterns were collected at 295 K with a step-scan procedure in the range of 2θ=10°~100°. The step interval was 0.02°, and the time per step was 1 s. The accelerating voltage and applied current were 40 kV and 40 mA, respectively. Fourier transform infrared spectroscopy (FTIR, Nexus, Nicolet Corporation, Madison, Wisconsin, USA) was applied to examine the FTIR spectra of Sm_2FeSbO_7. Its spectral range is between 7 400~350 cm^{-1} and the resolution is better than 0.09 cm^{-1}. The UV-visible diffuse reflectance spectrum of Sm_2FeSbO_7 was gauged with a Shimadzu UV-2550 UV-Visible spectrometer (Shimadzu, Santa Clara, California, USA), and $BaSO_4$ was utilized as the reference material.

1.3 Photocatalytic activity experiments

The photocatalytic activity of Sm_2FeSbO_7 was assessed with indigo carmine (IC) ($C_{16}H_8N_2Na_2O_8S_2$) (Tianjin Bodi Chemical Co., Ltd., Tianjin, China) as the model substance. The photoreaction was implemented in a photochemical reaction apparatus (Nanjing Xujiang Machine Plant, Nanjing, China). The inner structure of the reaction apparatus was as following: the lamp was put into a quartz hydrazine, which was a hollow structure, and lied in the middle of the reactor. The recycling water through the reactor kept at a near constant reaction temperature (20 ℃), and the solution was continuously stirred and aerated. Twelve holes were utilized to put quartz tubes evenly arranged around the lamp, and the distance between the lamp and each hole was equal. The photocatalyst within the IC solution was in a state of suspension under the condition of magnetic stirring. In this paper, the photocatalytic degradation of IC was carried out with 0.3 g Sm_2FeSbO_7 in a 300 mL, 29.3 μmol·L^{-1} IC aqueous solution in quartz tubes with 500 W xenon lamp (400 nm<λ<800 nm) as the visible light source. Prior to visible light irradiation, the suspensions which contained the catalyst and IC coloring matter, were magnetically stirred in darkness for 45 min to ensure the establishment of an adsorption/desorption equilibrium among Sm_2FeSbO_7, the IC coloring matter and atmospheric oxygen. During visible light illumination, the suspension was stirred at 500 r·s^{-1}, and the initial pH value of the IC solution was 7.0 without pH value adjustment in the reaction process. Above experiments were carried out under oxygen-saturation conditions ($c_{O_2, sat}$=1.02 mmol·L^{-1}). One of the quartz tubes was taken out from the photochemical reaction apparatus at various time intervals. The suspension was filtered through 0.22 μm membrane filters. The filtrate was subsequently analyzed by a Shimadzu UV-2450 spectrometer (Shimadzu, Santa Clara, California, USA) with a detecting wavelength at 610 nm.

The photonic efficiency (ξ) was calculated according to the following formula[43-44]:

$$\xi = R/I_0 \quad (1)$$

where ξ was the photonic efficiency (%), R was the degradation rate of IC ($mol \cdot L^{-1} \cdot s^{-1}$), which indicated the concentration decrement of indigo carmine within every second, and I_0 was the incident photon flux ($Einstein \cdot L^{-1} \cdot s^{-1}$). The incident photon flux, I_0, which was measured by a radiometer (Model FZ-A, Photoelectric Instrument Factory, Beijing Normal University, Beijing, China), was determined to be 4.76×10^{-6} $Einstein \cdot L^{-1} \cdot s^{-1}$ under visible light irradiation (a wavelength range of 400~700 nm).

2 Results and discussion

2.1 Crystal structure and optical properties

The transmission electron microscopy (TEM) image of the prepared catalyst, Sm_2FeSbO_7, is shown in Fig.1. It could be observed clearly from Fig.1a that the particles of Sm_2FeSbO_7 had a nanostructure and irregular shapes. Additionally, we could also acknowledge that the particles of Sm_2FeSbO_7 crystallized well. Fig.1b showed the selected area electron diffraction pattern of Sm_2FeSbO_7. It could be seen from Fig.1b that Sm_2FeSbO_7 crystallized with a pyrochlore-type structure, a cubic crystal system and a space group *Fd3m*. The results showed that the lattice parameters for Sm_2FeSbO_7 were proven to be $a=b=c=$ 1.035 434 nm. According to the calculation results from Fig.1b, the (*hkl*) value for the main peaks of Sm_2FeSbO_7 had been found and indexed.

Fig.2 presents the scanning electron microscopy-energy-dispersive spectrometry (SEM-EDS) spectrum of Sm_2FeSbO_7. Fig.2 indicated the presence of samarium, iron, antimony and oxygen element. In order to avoid the influence of inhomogeneity phenomenon on the selected surface, ten different specimen areas selection of Sm_2FeSbO_7 were conducted in an EDS test. The mean value of the results of above EDS spectra taken from prepared Sm_2FeSbO_7 indicated that the stoichiometric ratio of samarium, iron, antimony and oxygen was estimated to

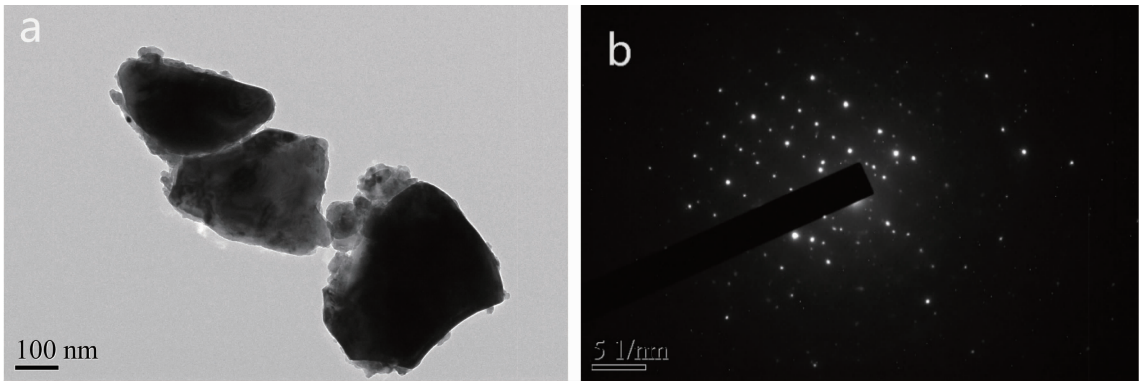

Fig.1　(a) TEM image of Sm_2FeSbO_7; (b) Selected area electron diffraction pattern of Sm_2FeSbO_7

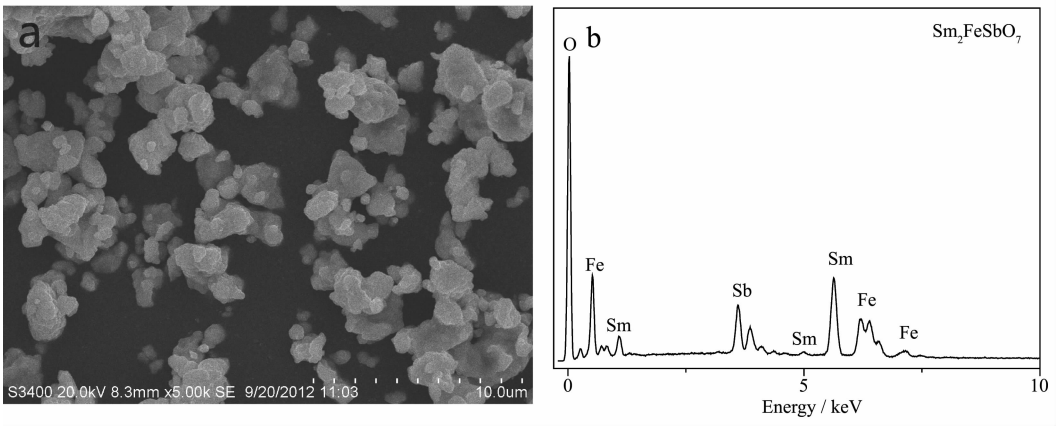

Fig.2　(a) SEM image of Sm_2FeSbO_7; (b) EDS spectrum of Sm_2FeSbO_7 calcinated at 800 ℃ for 35 h

be 17.61:9.34:7.97:65.09, namely 2.00:1.06:0.90:7.40.

In order to get a better understanding of the chemical state of all elements on the catalyst surface, the X-ray photoelectron spectroscopy (XPS) full spectrum of Sm_2FeSbO_7 was measured and was displayed in Fig.3. The experimental results showed that the XPS full spectrum of Sm_2FeSbO_7 contained only the corresponding elements and carbon element, and the carbon element was due to the addition of hydrocarbons which would facilitate the testing and calibration of the elements instead of a catalyst. Table 1 provides the experimental binding energy of the characteristic peaks of all elements which exist in Sm_2FeSbO_7 and the binding energy information after C correction. By comparing the XPS standard binding energy data shown in Table 1 and the chemical shifts of each element, the valence state of each element in Sm_2FeSbO_7 was determined, and the results showed that the valence state of Sm, Fe, Sb or O was +3, +3, +5 or −2.

Fig.4 shows the powder X-ray diffraction pattern of Sm_2FeSbO_7 with the full-profile structure refinements of the collected data. The collected data were obtained by the RIETAN™ [45] program based on the

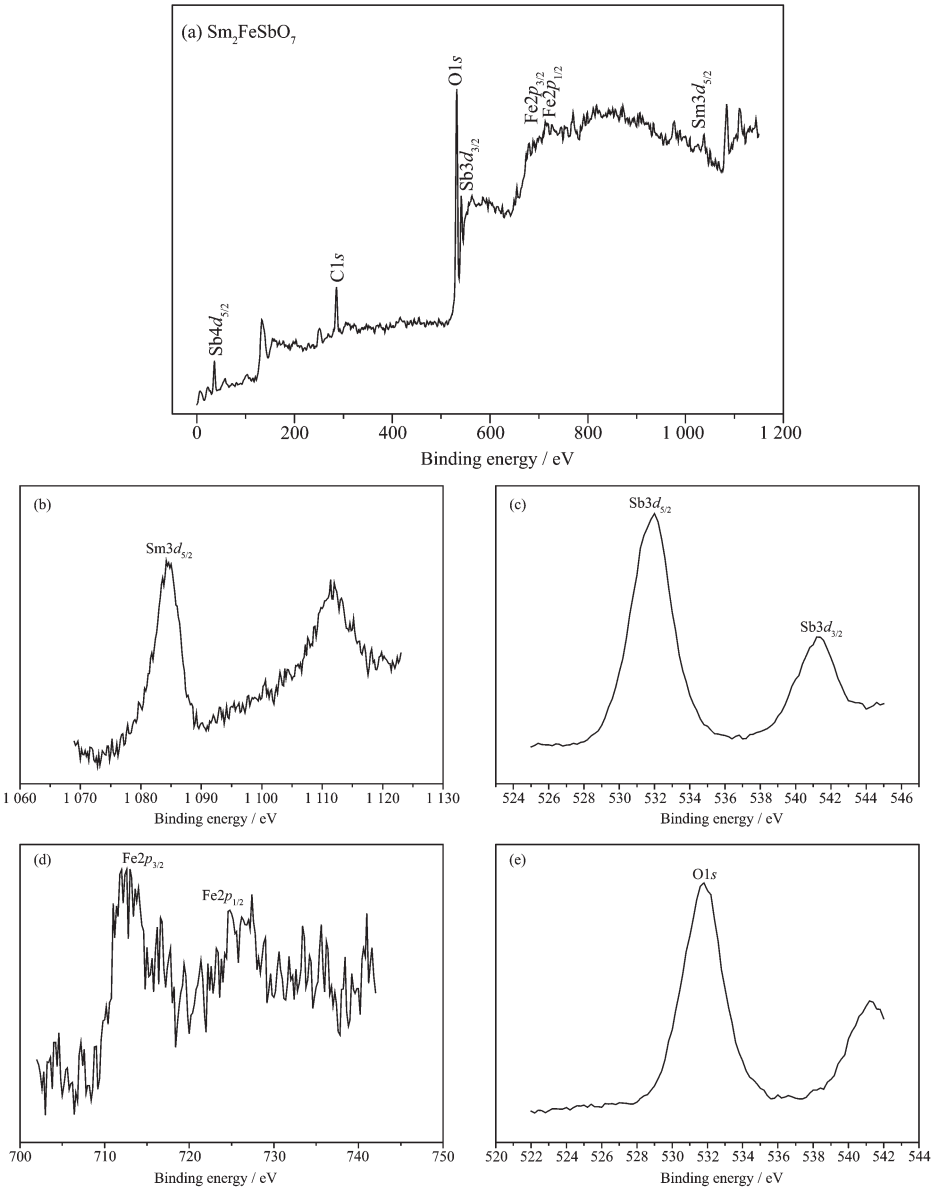

Fig.3 XPS spectra of Sm_2FeSbO_7 and every element which was contained in Sm_2FeSbO_7: (a) Full XPS spectrum of Sm_2FeSbO_7; XPS spectra of (b) Sm3$d_{5/2}$, (c) Sb3d, (d) Fe2p and (e) O1s

Table 1　Binding energies for key elements of Sm_2FeSbO_7

Element	Sm3$d_{5/2}$	Fe2$p_{1/2}$	Sb3$d_{5/2}$	O1s	C1s
Binding energy / eV	1 084.6	724.8	532.0	531.8	286.0
Binding energy after C correction / eV	1 083.1	723.3	530.5	530.3	284.5

Rietveld analysis. It could be seen from Fig.4 that Sm_2FeSbO_7 turned out to be a single phase. Additionally, the results of the final refinements for Sm_2FeSbO_7 indicated a good agreement between the observed intensities and the calculated intensities for a pyrochlore-type structure, a cubic crystal system and a space group *Fd*3*m* (O atoms were included in the model). The lattice parameters of Sm_2FeSbO_7 were $a=b=c=1.035\ 434$ nm. All the diffraction peaks of Sm_2FeSbO_7 could be successfully indexed according to the lattice constant and above refinement results as well as the space group *Fd*3*m*. The atomic coordinates and structural parameters of Sm_2FeSbO_7 are listed in Table 2. According to above results, the structural model of Sm_2FeSbO_7 which is simulated by Materials Studio software is demonstrated in Fig.5.

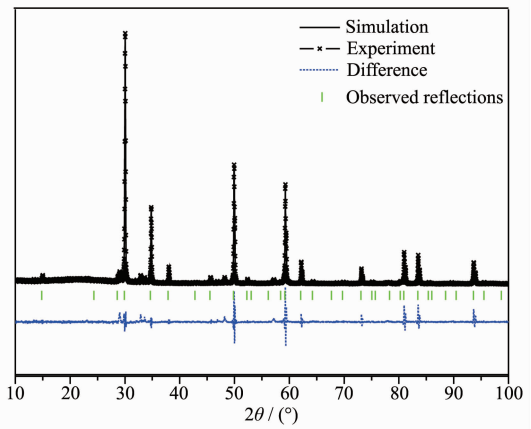

Fig.4　XRD patterns and Rietveld refinements of Sm_2FeSbO_7

Fourier transform infrared (FTIR) spectrum analysis of Sm_2FeSbO_7 particles is investigated in this study, as shown in Fig.6. According to Fig.6, we could find that the absorption bands of Sm_2FeSbO_7 prepared by a solid-state reaction method at 800 ℃ were at 487 and 625 cm^{-1}. The strong absorption band near 487 cm^{-1} should be attributed to the Sm-O vibration. The

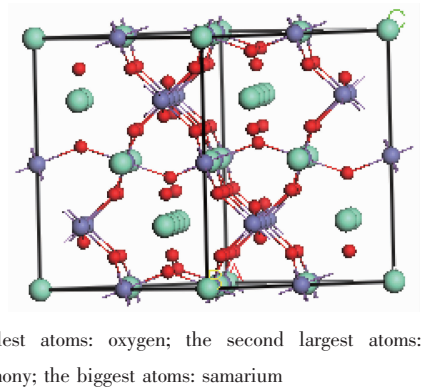

Smallest atoms: oxygen; the second largest atoms: iron and antimony; the biggest samarium

Fig.5　Structural model of Sm_2FeSbO_7 simulated by Materials Studio software corresponding to the XRD pattern shown in Fig.4

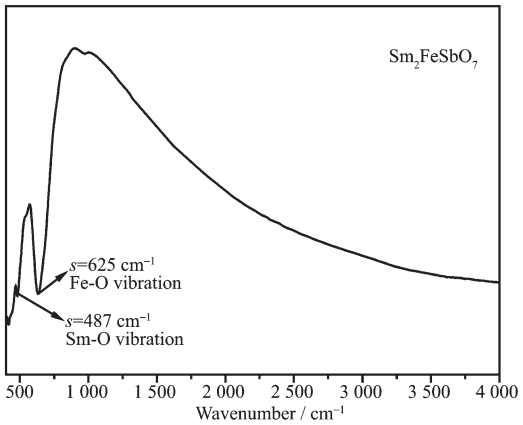

Fig.6　FTIR spectrum of Sm_2FeSbO_7 calcinated at 800 ℃ for 35 h

Table 2　Structural parameters of Sm_2FeSbO_7 calcinated at 800 ℃ for 35 h

Atom	x	y	z	Occupation factor
Sm	0	0	0	1
Fe	0.5	0.5	0.5	0.5
Sb	0.5	0.5	0.5	0.5
O(1)	−0.175	0.125	0.125	1
O(2)	0.125	0.125	0.125	1

absorption band which situated at 625 cm^{-1} was overlaid by the symmetric bending and stretching of the Fe-O which should be the Fe-O vibration.

The absorption spectrum of Sm_2FeSbO_7 is presented in Fig.7. For a crystalline semiconductor, the optical absorption near the band edge following Eq.(**2**)[46]:

$$\alpha h\nu = A(h\nu - E_g)^n \quad (2)$$

$$E_g = 1\ 240/\lambda \quad (3)$$

Where A, α, E_g, ν and λ were the proportional constant, absorption coefficient, band gap, light frequency and absorption edge, respectively. In this equation, n determined the character of the transition in a semiconductor. E_g and n could be calculated by the following steps[47]: (i) plotting $\ln(\alpha h\nu)$ versus $\ln(h\nu - E_g)$ by assuming an approximate value of E_g, which could be calculated by Eq.(**3**); (ii) deducing the value of n; and (iii) refining the value of E_g. From Fig.7, we could find that the absorption edge of Sm_2FeSbO_7 was about 461 nm, meaning that the estimated E_g of Sm_2FeSbO_7 was 2.69 eV. Then, from the plot of ln $(\alpha h\nu)$ versus ln $(h\nu - E_g)$, where we could find that the slope of the line part was about 1.27. Therefore, the n of Sm_2FeSbO_7 was 2. After plotting $(\alpha h\nu)^{1/2}$ versus $h\nu$ and extrapolating the plot to $(\alpha h\nu)^{1/2}=0$, the accurate value of E_g of Sm_2FeSbO_7 was calculated as 2.46 eV. Applying the same calculation process to N-TiO_2, we found that n was 2 for N-TiO_2 and the band gap E_g of N-TiO_2 was 2.76 eV. Above results indicated that the optical transition for Sm_2FeSbO_7 or N-TiO_2 was indirectly allowed, and Sm_2FeSbO_7 possessed a narrow band gap compared with N-TiO_2. The valence-band XPS spectra (Fig.8) showed that the valence band position of the sample had no obvious changes. According to the empirical equation:

$$E_{VBM} = E_{CBM} + E_g \quad (4)$$

where E_{VBM} and E_{CBM} were the valence band maximum position and conduction band minimum position, respectively. Based on above information, the schematics depiction of the band structures of Sm_2FeSbO_7 sample was illustrated in Fig.9. The position of the valence band was at 0.98 eV and the position of the conduction band was at 3.44 eV.

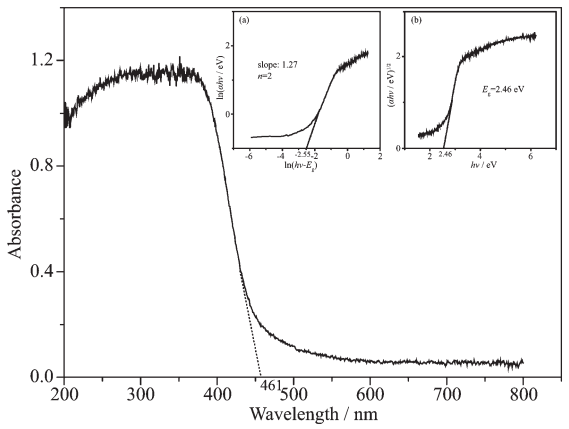

Inset: (a) is plot of $\ln(\alpha h\nu)$ versus $\ln(h\nu - E_g)$ and (b) is plot of $(\alpha h\nu)^{1/2}$ versus $h\nu$

Fig.7 Diffuse reflection spectra of Sm_2FeSbO_7

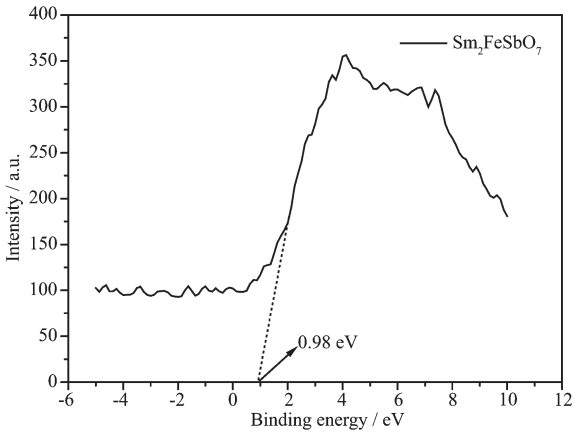

Fig.8 Valence band of Sm_2FeSbO_7

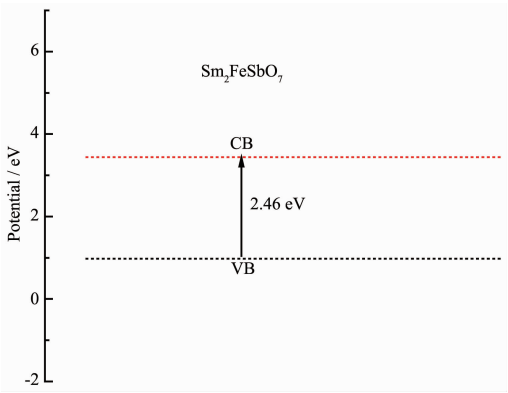

Fig.9 Suggested band structure of Sm_2FeSbO_7

2.2 Photocatalytic properties

The progress of photocatalysis using the semiconductor compound as catalyst could be described briefly as follows[48-49]. Firstly, the semiconductor compound absorbed photons, resulting in the generation of electron-hole pairs within the semiconductor

compound particles, subsequently, the diffusion of the charge carriers to the surface of the semiconductor compound particle would be followed; at the same time, the active sites of the surface of the semiconductor compound particles had been adsorbing a lot of organic pollutants particles; finally, the decomposition of the organic pollutants would be performed by charge carriers.

Fig.10 presents the changes in the UV-Vis spectra of IC under visible light irradiation (λ>420 nm) with the presence of Sm_2FeSbO_7. Above measurements were performed under oxygen-saturation conditions ($c_{O_2,\,sat}$=1.02 mmol·L^{-1}). It could be clearly noticed from Fig.10 that the typical IC peaks were at 609.5 nm. An obvious color change from deep blue into a colorless solution could be observed within 200 minutes. For further comparison, Fig.11 depicts the concentration changes of IC with Sm_2FeSbO_7 or nitrogen-doped TiO_2 (N-TiO_2) as photocatalyst under visible light irradiation, respectively.

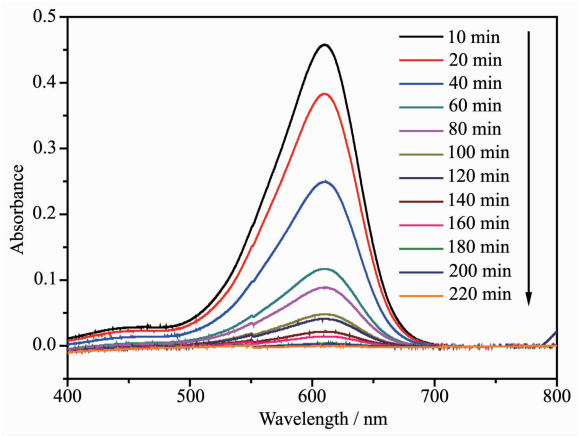

Fig.10　Spectral changes of aqueous solutions of indigo carmine due to visible light irradiation with the presence of Sm_2FeSbO_7 calcinated at 800 ℃ for 35 h

It could be seen from Fig.11 that the photonic efficiency (λ=420 nm) was estimated to be 5.13×10^{-4} or 2.58×10^{-4} with Sm_2FeSbO_7 or N-TiO_2 as catalyst, respectively. When N-TiO_2 was utilized as a catalyst, the photodegradation conversion rate of IC was 55.39% after visible light irradiation for 220 minutes, while the indigo carmine was completely degradated by Sm_2FeSbO_7. The results showed that the photodegradation rate of IC and the photonic efficiency with Sm_2FeSbO_7 as a catalyst were both higher than those with N-TiO_2 as a catalyst. Above results showed that complete removal of indigo carmine was observed after visible light irradiation for 200 minutes with Sm_2FeSbO_7 as a catalyst. Besides, based on the absorbance changes of IC with light irradiation time, the kinetic curves of IC degradation under visible light irradiation were figured out. Above results demonstrated that the photocatalytic kinetics of IC degradation with Sm_2FeSbO_7 or N-TiO_2 as photocatalyst followed a first order nature. The first-order rate constant for IC degradation was estimated to be 0.024 65 min^{-1} or 0.003 77 min^{-1} with Sm_2FeSbO_7 or N-TiO_2 as catalyst, respectively. This fact indicated that Sm_2FeSbO_7 was more efficient than N-TiO_2 for the photocatalytic degradation of IC under visible light irradiation.

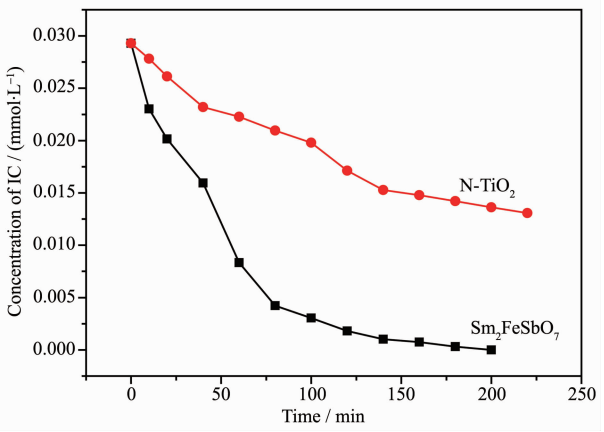

Fig.11　Photocatalytic degradation of indigo carmine under visible light irradiation with the presence of Sm_2FeSbO_7 or N-TiO_2 as photocatalyst, respectively

Fig.12 shows the change of total organic carbon (TOC) during the photocatalytic degradation of IC with Sm_2FeSbO_7 or N-TiO_2 as catalyst under visible light irradiation. TOC was measured using a TOC detector (TOC, vario TOC, Elementar, German). It has a detection limit of 2 μg·L^{-1} and an accuracy of RSD (C)< 1%. The TOC measurements revealed the disappearance of organic carbon when the IC solution which contained Sm_2FeSbO_7 or N-TiO_2 was exposed under visible light irradiation. The results showed that

53.26% of a TOC decrease was obtained after visible light irradiation for 220 minutes when N-TiO_2 was utilized as the photocatalyst, while TOC was completely removed by Sm_2FeSbO_7. The apparent first order rate constant k was estimated to be 0.021 57 or 0.003 64 min^{-1} with Sm_2FeSbO_7 or N-TiO_2 as the photocatalyst, respectively.

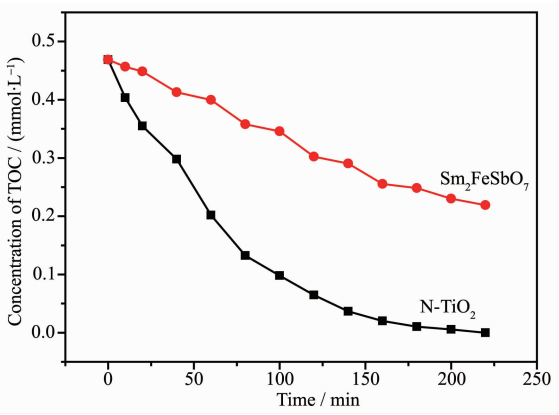

Fig.12 TOC plots during the photocatalytic degradation of indigo carmine under visible light irradiation with Sm_2FeSbO_7 or N-TiO_2 as photocatalyst, respectively

We used a carbon dioxide detector (B1040, WOST, Shenzhen, China) to quantitatively measure the concentration of carbon dioxide. Fig.13 presents the CO_2 yield during the photocatalytic degradation of IC with Sm_2FeSbO_7 or N-TiO_2 as the photocatalyst under visible light irradiation. During the progress of IC degradation, IC was converted into smaller organic species and was ultimately mineralized to inorganic products, such as carbon dioxide and water. The amount of CO_2 increased gradually with increasing reaction time when IC was photodegraded with Sm_2FeSbO_7 or N-TiO_2 as the photocatalyst. The results showed that the production rate of CO_2 from the Sm_2FeSbO_7-IC system was higher than that from the N-TiO_2-IC system with increasing reaction time. For example, the production amount of CO_2 was 0.074 61 mmol with N-TiO_2 as the photocatalyst after a visible light irradiation of 220 minutes. However, the production amount of CO_2 was 0.140 33 mmol with Sm_2FeSbO_7 as the photocatalyst after a visible light irradiation of 220 minutes.

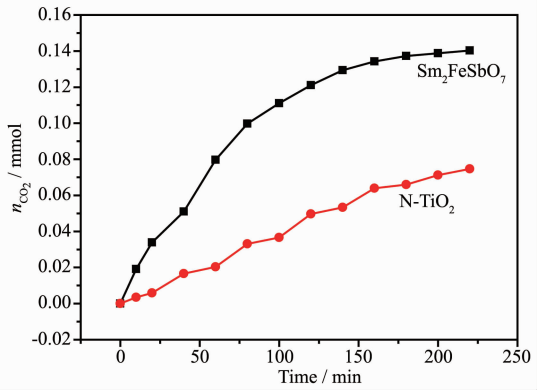

Fig.13 CO_2 production during the photocatalytic degradation of indigo carmine with Sm_2FeSbO_7 or N-TiO_2 as photocatalyst respectively under visible light irradiation

The first order nature of the photocatalytic degradation kinetics with Sm_2FeSbO_7 or N-TiO_2 as catalyst is clearly exhibited in Fig.14, which presents

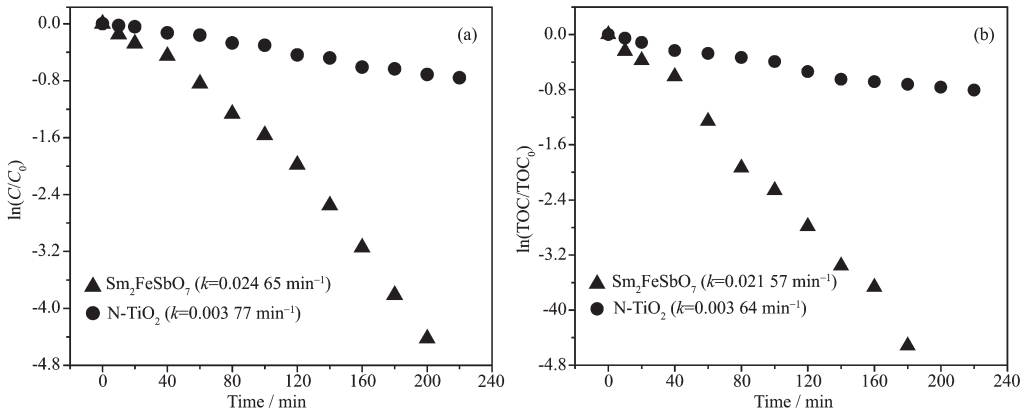

(a) Concentration; (b) Total organic carbon

Fig.14 Observed first order kinetic plots for the photocatalytic degradation of IC with Sm_2FeSbO_7 or N-TiO_2 as catalyst under visible light irradiation

a linear correlation between $\ln(C/C_0)$ (or $\ln(TOC/TOC_0)$) and the visible light irradiation time for the photocatalytic degradation of IC with the presence of the photocatalyst. In above equation, C represents the IC concentration at time t, and C_0 represents the initial IC concentration, and TOC represents the total organic carbon concentration at time t, and TOC_0 represents the initial total organic carbon concentration. According to the relationship between $\ln(C/C_0)$ and the light irradiation time, the apparent first order rate constant k was 0.024 65 min^{-1} with Sm_2FeSbO_7 as catalyst and 0.003 77 min^{-1} with N-TiO_2 as catalyst, indicating that Sm_2FeSbO_7 was more efficient than N-TiO_2 for the photocatalytic degradation of IC under visible light irradiation. According to the relationship between $\ln(TOC/TOC_0)$ and the light irradiation time, the apparent first order rate constant k_{TOC} was estimated to be 0.021 57 min^{-1} with Sm_2FeSbO_7 as catalyst and 0.003 64 min^{-1} with N-TiO_2 as catalyst, indicating that the photodegradation intermediate products of IC probably appeared during the photocatalytic degradation of IC under visible light irradiation.

In order to explore the mechanism of the IC degradation with Sm_2FeSbO_7 or N-TiO_2 as photocatalyst under visible light irradiation, we also test the concentration of NO_3^- and SO_4^{2-}, which are shown in Fig.15 and Fig.16, which may be formed as the end products of nitrogen atoms and sulfur atoms that exist in IC. From Fig.15 and Fig.16 we could be sure that both NO_3^- and SO_4^{2-} appeared during IC degradation with Sm_2FeSbO_7 or N-TiO_2 as the photocatalyst. NO_3^- and SO_4^{2-} ions were generated more quickly and effectively with Sm_2FeSbO_7 as photocatalyst compared with NO_3^- and SO_4^{2-} ions which were generated with N-TiO_2 as photocatalyst, which was in accord with above analysis about the degradation progress of IC. According to the NO_3^- concentration in Fig.15, we could calculate that 92.82% or 41.89% of nitrogen from IC was converted into nitrate ions with Sm_2FeSbO_7 or N-TiO_2 as the photocatalyst after visible light irradiation for 220 minutes. Meanwhile, it could be also concluded form Fig.14 that 72.24% or 39.11% of sulfur from IC was converted into sulfate ions with Sm_2FeSbO_7 or N-TiO_2 as photocatalyst after visible light irradiation for 220 minutes. It was noteworthy that the amount of SO_4^{2-} or NO_3^- which was released into the solution was sharply lower than the stoichiometry value of 100%. One possible reason could be a loss of sulfur-containing volatile compounds or SO_2 for the S element and nitrogen-containing volatile compounds or NH_3 for the N element. The second possible reason was a partially irreversible adsorption of some SO_4^{2-} and NO_3^- on the surface of the photocatalyst, which had been observed by Lachheb et al. with titanium dioxide[50].

In order to investigate the effect of the photosensitivity on the degradation process, we used

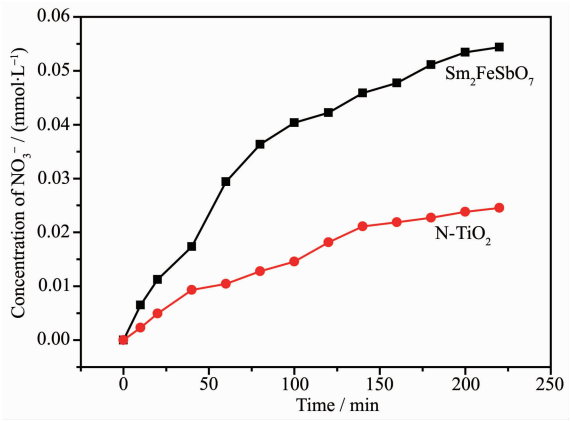

Fig.15　NO_3^- production during the photocatalytic degradation of IC with Sm_2FeSbO_7 or N-TiO_2 as photocatalyst respectively under visible light irradiation

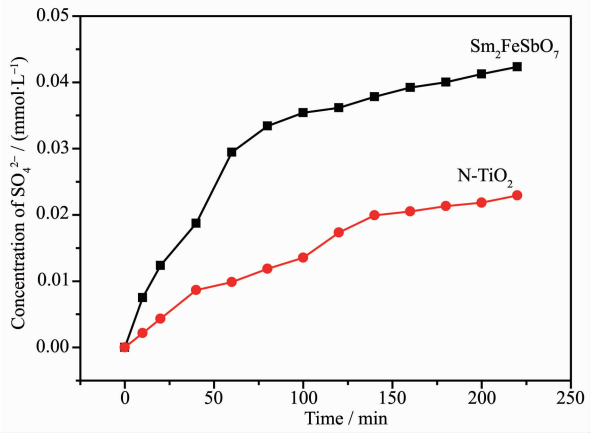

Fig.16　SO_4^{2-} production during the photocatalytic degradation of IC with Sm_2FeSbO_7 or N-TiO_2 as photocatalyst respectively under visible light irradiation

phenol as a contaminant for degradation of IC. Fig.17 shows the photocatalytic degradation of phenol with Sm_2FeSbO_7 as a photocatalyst under visible light irradiation. The concentration of phenol was determined by high performance liquid chromatography (HPLC, Agilent 1200-DAD, Agilent Technologies Co. Ltd., Palo Alto, USA). It was obvious to discover that the photocatalytic activity was acquired while colorless phenol was selected as a contaminant model with Sm_2FeSbO_7 as photocatalyst. The photocatalytic degradation efficiency of phenol was estimated to be 97.22% by Sm_2FeSbO_7 under visible light irradiation after 200 minutes, demonstrating that Sm_2FeSbO_7 itself had photocatalytic activity and the photosensitive effect was not the main factor in the photodegradation process of IC by using Sm_2FeSbO_7 as a photocatalyst.

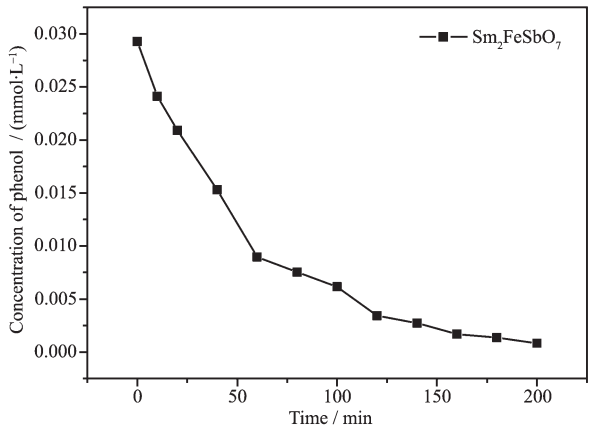

Fig.17 Photocatalytic degradation of phenol under visible light irradiation with Sm_2FeSbO_7 as photocatalyst

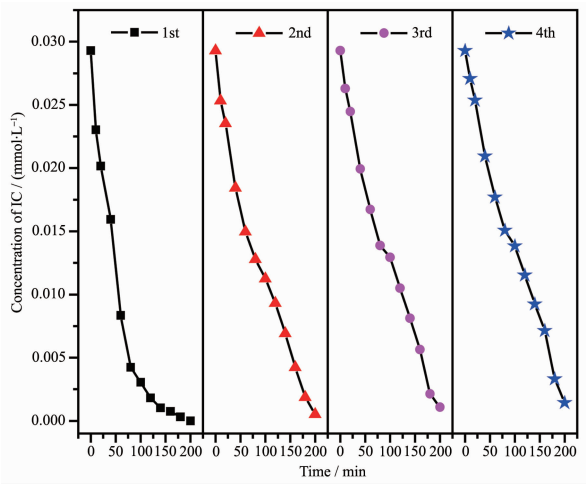

Fig.18 Repeated photocatalytic degradation tests of IC by Sm_2FeSbO_7

In order to probe the stability of the catalyst Sm_2FeSbO_7, we carried out an experiment of repeated degradation of IC. Fig.18 shows the experimental results of repeated degradation of IC under the same experimental conditions after four times of Sm_2FeSbO_7 recovery. The results showed that the removal rates of IC were 97.99%, 97.69%, 97.02% and 96.62% respectively after four reuses of Sm_2FeSbO_7. Though the degradation effect decreased slightly each time, it had a good performance with high degradability. It could be inferred that the catalytic performance of Sm_2FeSbO_7 is relatively stable and repeatable.

2.3 Photocatalytic degradation pathway of IC with Sm_2FeSbO_7 as photocatalyst

Fig.19 manifests the graphical representations of the relative distributions of the intermediate product as a function during the photodegradation of IC. The intermediates which were generated during the degradation process of IC were detected and identified by comparison with commercial standard samples. The intermediates in our experiment were identified as follows: indigotin, isatin sulfonic acid, 2-nitrobenzoic acid, indole-2,3-dione, *o*-nitrobenzaldehyde, nitro-acetophenone, anthranilic acid, oxalic acid, formic acid and acetic acid. The sulfur element was first hydrolytically removed and subsequently was oxidized and transformed into SO_4^{2-}. At the same time, nitrogen atoms in the −3 oxidation state produced NH_4^+ cations which subsequently were oxidized into NO_3^- ions. Moreover, carbon and oxygen elements were turned

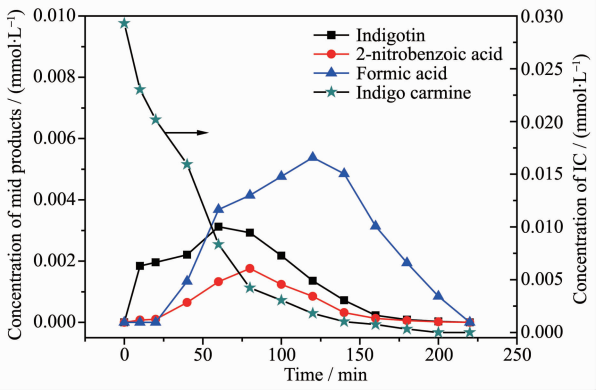

Fig.19 Temporal change in the distribution of the intermediates during the photodegradation of IC

into carbon dioxide. Accompanied by the rapid decomposition of IC, the concentration of other intermediate products first increased and then decreased by ulteriorly light irradiation, which uncovered the formation and the conversion of the reactive intermediate products. As the starts of the illumination reaction, the concentration of the three intermediates indigotin, 2-nitrobenzoic acid and formic acid gradually increased and subsequently decreased after reaching the highest concentration point. Indigotin was first detected in the second minute and reached the top concentration in the sixtieth minute. 2-nitrobenzoic acid was detected in the tenth minute and peaked in the eightieth minute. Formic acid was detected finally in the twenty-fifth minute and peaked in the one hundred and twentieth minute. And formic acid was the last intermediate product to disappear. Above results indicated that during the degradation process of IC, indigotin was formed firstly, subsequently 2-nitrobenzoic acid produced secondly, ultimately formic acid was detected thirdly. These intermediate products would be further degraded into small molecules. Above variations unambiguously uncovered that the decomposition of IC was a stepwise course.

Based on above results, combined with the analysis of the software simulations and experimental data, we can narrow down the degradation path of IC to a certain extent and arrive at the most likely degradation pathway of IC with Sm_2FeSbO_7 as catalyst, as shown in Fig.20. This pathway was similar to the

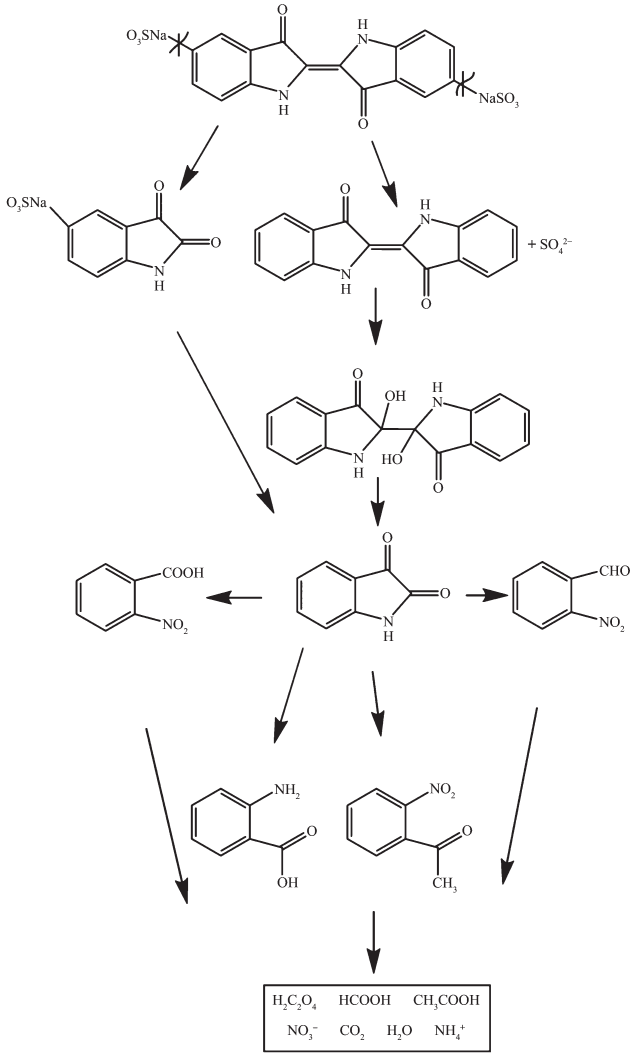

Fig.20　Suggested photocatalytic degradation pathway scheme for indigo carmine under visible light irradiation with the presence of Sm_2FeSbO_7 prepared by a solid-state reaction method at 800 ℃ for 35 h

pathway proposed by Zhang et al.[51] and Qu et al.[52]. According to Fig.20 the main degradation end products of IC were CO_2, H_2O, NO_3^- and SO_4^{2-}.

2.4 Photocatalytic degradation mechanism

We could easily Figure out that the organic pollutants can be degraded by the photogenerated reactive species during the photocatalytic reaction, including holes (h^+), electrons (e^-), hydroxyl radicals ($\cdot OH$) and superoxide radicals ($\cdot O_2^-$). In order to verify the major reactive species for inducing the degradation of IC with Sm_2FeSbO_7 as catalyst under visible light irradiation, dissociative scavenger experiments were demonstrated by adding different scavengers into the system. Superoxide dismutase (SOD) with the concentration of 66.7 mg·L^{-1}, ethylene diamine tetraacetic acid (EDTA) with the concentration of 10 mmol·L^{-1}, $AgNO_3$ with the concentration of 10 mmol·L^{-1} and *tert*-butyl alcohol (TBA) with the concentration of 10 mmol·L^{-1} were added into the system as scavengers to capture $\cdot O_2^-$, h^+, e^- and $\cdot OH$, respectively. The photodegradation of indigo carmine over Sm_2FeSbO_7 in the face of various scavengers are expounded in Fig.21. As shown in Fig.21, after the addition of $AgNO_3$ as a scavenger for photogenerated electrons (e^-), the photodegradation efficiency of IC remained almost the same compared with the system of no scavenger, demonstrating the minor role of e^- in this photocatalytic reaction process. When TBA was used as the scavenger to eliminate $\cdot OH$, the photodegradation activity declined somewhat. Moreover, an obvious reduction in the photocatalytic performance was observed in the presence of SOD or EDTA, which eliminated $\cdot O_2^-$ or h^+. Above results suggested that the photoreaction process was dominated by h^+ and $\cdot O_2^-$ in this system because of their considerable impact. We could derive that h^+ contributed most to the high activity of Sm_2FeSbO_7 during the degradation of IC in the former most of the time. Additionally, $\cdot O_2^-$ radicals had a high importance during IC degradation. As for $\cdot OH$ radicals, they might participate in the photodegradation process with slight catalytic activity. However, e^- showed almost no activity during the degradation of IC in the presence of Sm_2FeSbO_7.

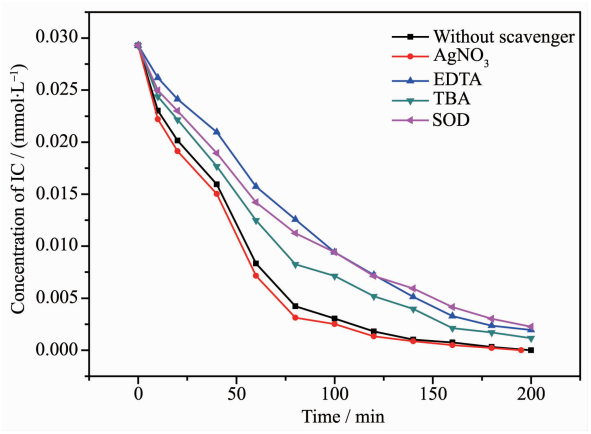

Fig.21 Photodegradation of indigo carmine over Sm_2FeSbO_7 without scavenger and in the presence of various scavengers of EDTA, SOD, $AgNO_3$ and TBA

Based on above results, a possible mechanism scheme of the charge separation and photocatalytic reaction for Sm_2FeSbO_7 is shown in Fig.22. Firstly, photoinduced holes (h^+) and photoinduced electrons (e^-) came into being in the surface of Sm_2FeSbO_7 particles (Eq. (**5**)). Secondly, organic pollutants (R) could be degraded into inorganic products with the effluence of h^+ and e^-. Many published works [53-55] had confirmed that two oxidative agents could be mainly concerned under visible light irradiation: $\cdot OH$ radicals and $\cdot O_2^-$ radicals. Then h^+ reacted with R directly (Eq. (**6** ~**8**)). Besides, the effect of dye sensitization should be taken into consideration (Eq.(**9**~**10**), IC*: IC in the excited state, IC^+: hole containing IC), because IC could be excited by visible light irradiation, subsequently, the sensitizing dye molecules injected electrons into the semiconductor nanocrystallites,

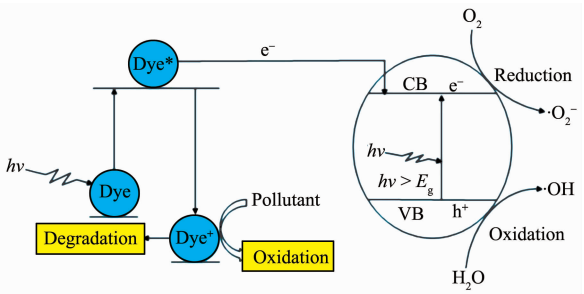

CB: Conduction band; VB: Valence band

Fig.22 Suggested photodegradation reaction mechanism of indigo carmine with Sm_2FeSbO_7 as the photocatalyst under visible light irradiation

which were collected at a conducting surface to generate the photocurrent (Eq.(**11**))[56-57].

$$Sm_2FeSbO_7+h\nu \rightarrow h^++e^- \quad (\mathbf{5})$$

$$(H_2O \rightleftharpoons H^++OH^-)+h^+ \rightarrow H^++\cdot OH \quad (\mathbf{6})$$

$$O_2+e^- \rightarrow \cdot O_2^- \quad (\mathbf{7})$$

$$R+\cdot OH/\cdot O_2^-/h^+ \rightarrow \text{intermediates} \rightarrow \text{degradation products} \quad (\mathbf{8})$$

$$IC+h\nu \rightarrow IC^* \quad (\mathbf{9})$$

$$IC^*+Sm_2FeSbO_7 \rightarrow IC^++Sm_2FeSbO_7(e^-) \quad (\mathbf{10})$$

$$Sm_2FeSbO_7(e^-)+O_2 \rightarrow O_2^-+Sm_2FeSbO_7 \quad (\mathbf{11})$$

The M-O-M bond angle was closer to 180°, and the excited state was more delocalized as shown by previous study[58], thus the charge carriers could move easily in the matrix. High diffusivity due to the mobility of the photoinduced electrons and the photoinduced holes helped impel more electrons and holes to reach the reactive sites on the catalyst surface, therefore the photon efficiency of Sm_2FeSbO_7 was improved. The Sm-O-Sm bond angle of Sm_2FeSbO_7 was 180° and the Sb-O-Sb bond angle of Sm_2FeSbO_7 was 139.624° which was close to 180°. Thus, the photocatalytic activity of Sm_2FeSbO_7 was correspondingly higher. The crystal structures of Sm_2FeSbO_7 and N-doped TiO_2 were diverse, subsequently the electronic structures of Sm_2FeSbO_7 and N-doped TiO_2 were diverse, either. For Sm_2FeSbO_7, Sm was 6*f*-block metal element, and Fe was 4*d*-block metal element, and Sb was 5*p*-block metal element. Moreover, for N-doped TiO_2, Ti was 4*d*-block metal element, indicating that the photocatalytic activity might be affected by not only the crystal structure but also the electronic structure of the photocatalyst. The difference of the photocatalytic degradation activity of IC among Sm_2FeSbO_7 and N-doped TiO_2 could be attributed mainly to the difference of their crystalline and electronic structures.

3 Conclusions

In summary, newly synthesized photocatalyst Sm_2FeSbO_7 was prepared for the first time. Sm_2FeSbO_7 showed higher photocatalytic activity compared with N-doped TiO_2 for the photocatalytic degradation of indigo carmine under visible light irradiation and the structural properties of Sm_2FeSbO_7 was characterized by some material characterization methods. The XRD results showed that Sm_2FeSbO_7 owned a pyrochlore-type structure, a cubic crystal system and a space group *Fd*3*m*. The lattice parameters of Sm_2FeSbO_7 were $a=b=c=1.035\ 434$ nm. XPS results of Sm_2FeSbO_7 indicated that the valence state of Sm, Fe, Sb or O was +3, +3, +5 or −2. The photocatalytic decomposition of IC aqueous solution was realized under visible light irradiation in the presence of Sm_2FeSbO_7 or N-doped TiO_2. The results could apparently state that the photodegradation rate of IC and the photonic efficiency with Sm_2FeSbO_7 as catalyst was higher than those with N-doped TiO_2 as catalyst, which illustrated that Sm_2FeSbO_7 exhibited higher photocatalytic activities for IC degradation under visible light irradiation compared with N-doped TiO_2. The photocatalytic degradation of indigo carmine with Sm_2FeSbO_7 as a catalyst followed the first-order reaction kinetics. The obvious first-order rate constant of Sm_2FeSbO_7 or N-doped TiO_2 was 0.024 65 or 0.003 77 min^{-1}. During the photocatalytic process, the reduction of the total organic carbon, formation of inorganic products such as SO_4^{2-} and NO_3^-, and the evolution of CO_2 uncovered the continuous mineralization of IC. The experimental results of degradation of phenol by Sm_2FeSbO_7 demonstrated that the photosensitive effect was not the main factor in the photodegradation process of IC, and it possessed excellent repeatability. The possible photocatalytic degradation pathway of indigo carmine was obtained. The results which were obtained in our investigations proved that Sm_2FeSbO_7 (visible light) photocatalysis might be regarded as a method for the practical treatment of diluted colored waste water in the environment of room-temperature and ordinary pressure.

Acknowledgments: This work was supported by a grant from the fifth group of China-Israel Joint Research Program in Water Technology and Renewable Energy (Grant No.[2010]30) and the National Natural Science Foundation of China (Grant No.21277067).

Author Contributions: LUAN Jing-Fei was involved with all aspects of the work including visualizing, planning, and data explication. TAN Wen-Cheng carried out the experiments, analyzed the data and wrote the paper. All authors read and approved the manuscript.

Conflicts of Interest: The authors declare no conflict of interest.

References:

[1] Song Y L, Li J T, Bo B. *Water Air Soil Pollut.*, **2010**,**213**(1/2/3/4):311-317

[2] Wang S B, Li H T. *J. Hazard. Mater.*, **2005**,**126**:71-77

[3] Xu L, Wei Y G, Guo W, et al. *Appl. Surf. Sci.*, **2015**,**332**:682-693

[4] Zhang M Y, Shao C L, Guo Z C, et al. *ACS Appl. Mater. Interfaces*, **2011**,**3**:2573-2578

[5] Wang J, Li J, Zhang L Q, et al. *Catal. Lett.*, **2009**,**130**(3/4):551-557

[6] Du H Y, Luan J F. *Solid State Sci.*, **2012**,**14**:1295-1305

[7] Benshahar Y, Banin U. *Top. Curr. Chem.*, **2016**,**374**(4):149-174

[8] Ahmad M, Ahmed E, Zhang Y W, et al. *Curr. Appl. Phys.*, **2013**,**13**(4):697-704

[9] Yao W F, Ye J H. *Catal. Lett.*, **2006**,**110**(1/2):139-142

[10]Pena M E, Korfiatis G P, Patel M, et al. *Water Res.*, **2005**, **39**(11): 2327-2337

[11]Pham T D, Lee B K. *Appl. Surf. Sci.*, **2014**,**296**:15-23

[12]Josephine G A S, Ramachandran S, Sivasamy A. *J. Saudi Chem. Soc.*, **2015**,**19**(5):549-556

[13]Li J L, Liu T, Sui G Z, et al. *J. Nanosci. Nanotechnol.*, **2015**, **15**(2):1408-1415

[14]Chai Y Y, Wang L, Ren J. *Appl. Surf. Sci.*, **2015**,**324**(45):212-220

[15]Yan C Y, Yi W T, Yuan H M, et al. *Environ. Prog. Sustainable Energy*, **2014**,**33**(2):419-429

[16]Wen X J, Niu C G, Min R, et al. *J. Colloid Interface Sci.*, **2017**,**497**:368-377

[17]Liang H R, Guo L J. *Int. J. Hydrogen Energy*, **2010**,**35**(13):7104-7109

[18]Song L M, Zhang S J, Chen B. *Catal. Commun.*, **2009**,**10**(12):1565-1568

[19]Luan J F, Zheng S R, Hao X P, et al. *J. Braz. Chem. Soc.*, **2006**,**17**(7):1368-1376

[20]Long M, Cai J, Cai W M, et al. *Prog. Chem.*, **2006**,**18**(9):1065-1075

[21]Rawal S B, Bera S, Lee W I. *Catal. Lett.*, **2012**,**142**:1482-1488

[22]Habibi-Yangjeh A, Shekofteh-Gohari M. *Sep. Purif. Technol.*, **2017**,**184**:334-346

[23]Kalantari K, Ahmad M B, Masoumi H R, et al. *Int. J. Mol. Sci.*, **2014**,**15**(7):12913-12927

[24]Vadivel S, Maruthamani D, Habibi-Yangjeh A, et al. *J. Colloid Interface Sci.*, **2016**,**480**:126-136

[25]Huang L Z, Liu B S. *RSC Adv.*, **2016**,**6**(22):17873-17879

[26]Chakraborty A K, Kebede M A. *React. Kinet., Mech Catal.*, **2012**,**106**(1):83-98

[27]Chai B, Peng T Y, Mao J, et al. *Phys. Chem. Chem. Phys.*, **2012**,**14**:16745-16752

[28]Bi J H, Fang W, Li L, et al. *J. Alloys Compd.*, **2015**,**649**:28-34

[29]Gouvêa C A, Wypych F, Moraes S G, et al. *Chemosphere*, **2000**,**40**(4):427-432

[30]Tatsuma T, Saitoh S, Ngaotrakanwiwat P, et al. *Langmuir*, **2002**,**18**:7777-7779

[31]Ullah K, Meng Z D, Ye S, et al. *J. Ind. Eng. Chem.*, **2014**,**20**(3):1035-1042

[32]Zhou J K, Zou Z G, Ray A K, et al. *Ind. Eng. Chem. Res.*, **2007**,**46**:745-749

[33]Zhang X, Ai Z H, Jia F L, et al. *Mater. Chem. Phys.*, **2007**, **103**:162-167

[34]Zhang G K, Zou X, Gong J, et al. *J. Alloys Compd.*, **2006**, **425**:76-80

[35]Farrukh M A, Imran F, Ali S, et al. *Russ. J. Appl. Chem.*, **2015**,**88**(9):1523-1527

[36]Ghorai T K, Chakraborty M, Pramanik P. *J. Alloys Compd.*, **2011**,**509**(32):8158-8164

[37]Xie L J, Ma J F, Xu G J. *Mater. Chem. Phys.*, **2008**,**110**:197-200

[38]Li X K, Kako T, Ye J H. *Appl. Catal., A*, **2007**,**326**:1-7

[39]Shetty K, Prathibha B S, Rangappa D, et al. *Mater. Today*, **2017**,**4**(11):11764-11772

[40]Jiang Y Y, Zhang J W, Hu Z Q, et al. *Appl. Mech. Mater.*, **2014**,**455**:99-105

[41]Chen C H, Liang Y H, Zhang W D. *J. Alloys Compd.*, **2010**, **501**:168-172

[42]Qiu J X, Wang C Y, Gu M Y. *Mater. Sci. Eng. B*, **2004**,**112**:1-4

[43]Marugan J, Hufschmidt D, Sagawe G, et al. *Water Res.*, **2006**,**40**:833-839

[44]Sakthivel S, Shankar M V, Palanichamy M, et al. *Water Res.*, **2004**,**38**:3001-3008

[45]Izumi F. *Rigaku J.*, **1989**,**6**(1):10-20

[46]Tauc J, Grigorovici R, Vancu A. *Phys. Status Solidi*, **1966**,**15**: 627-637

[47]Luan J F, Wang S, Ma K, et al. *J. Phys. Chem. C*, **2010**, **114**:9398-9407

[48]Yang Y J, Luan J F. *Molecules*, **2012**,**17**:2752-2772

[49]Chang M J, Wang H, Li H L, et al. *J. Mater. Sci.*, **2018**,**53**: 3682-3691

[50]Lachheb H, Puzenat E, Houas A, et al. *Appl. Catal., B*, **2002**, **39**:75-90

[51]ZHANG Xiao-He(张笑河), CHEN Guo-Qing(陈国庆), MA Chao-Qun(马超群). *Laser and Optoelectronics Progress*(激光与光电子学进展), **2018**,**55**(1):013007(5 Pages)

[52]Qu R J, Xu B Z, Meng L J, et al. *Water Res.*, **2015**,**68**:316-327

[53]Huang S Q, Xu Y G, Xie M, et al. *Colloids Surf. A*, **2015**, **478**(ISSN):71-80

[54]Subash B, Krishnakumar B, Swaminathan M, et al. *Langmuir*, **2013**,**29**:939-949

[55]Sun H Q, Zhou G L, Liu S Z, et al. *Chem. Eng. J.*, **2013**, **231**(9):18-25

[56]Ding H M, Sun H, Shan Y K. *J. Photochem. Photobiol. A*, **2005**,**169**:101-107

[57]Gadhi T A, Hernández-Gordillo A, Bizarro M, et al. *Ceram. Int.*, **2016**,**42**(11):13065-13073

[58]Wiegel M, Middel W, Blasse G. *J. Mater. Chem.*, **1995**,**5**(7): 981-983